Femtosecond single-electron pulses generated by two-photon photoemission close to the work function

2015 New J. Phys. 17 033008

(http://iopscience.iop.org/1367-2630/17/3/033008)

New Journal of Physics
The open access journal at the forefront of physics

Deutsche Physikalische Gesellschaft DPG
IOP Institute of Physics

Published in partnership with: Deutsche Physikalische Gesellschaft and the Institute of Physics

OPEN ACCESS

RECEIVED
11 November 2014

REVISED
23 December 2014

ACCEPTED FOR PUBLICATION
4 February 2015

PUBLISHED
3 March 2015

PAPER

Femtosecond single-electron pulses generated by two-photon photoemission close to the work function

L Kasmi[1,2], **D Kreier**[1,2], **M Bradler**[3], **E Riedle**[3] **and P Baum**[1,2]

[1] Ludwig-Maximilians-Universität München, Am Coulombwall 1, D-85748 Garching, Germany
[2] Max-Planck-Institut für Quantenoptik, Hans-Kopfermann-Str. 1, D-85748 Garching, Germany
[3] Lehrstuhl für BioMolekulare Optik, Ludwig-Maximilians-Universität München, Oettingenstr. 67, D-80538 München, Germany

E-mail: peter.baum@lmu.de

Keywords: ultrafast electron diffraction, 4D imaging, femtosecond electron microscopy, photoelectric effect

Abstract

Diffraction and microscopy with ultrashort electron pulses can reveal atomic-scale motion during matter transformations. However, the spatiotemporal resolution is significantly limited by the achievable quality of the electron source. Here we report on the emission of femtosecond single/few-electron pulses from a flat metal surface via two-photon photoemission at 50–100 kHz. As pump we use wavelength-tunable visible 40 fs pulses from a noncollinear optical parametric amplifier pumped by a picosecond thin-disk laser. We demonstrate the beneficial influence of photon energies close to the photocathode's work function for the coherence and duration of the electron pulses. The source's stability approaches the shot noise limit after removing second-order correlation with the driving laser power. Two-photon photoemission offers genuine advantages in minimizing emission duration and effective source size directly at the location of photoemission. It produces an unprecedented combination of coherent, ultrashort and ultrastable single/few-electron wave packets for time-resolving structural dynamics.

1. Introduction

The direct visualization of atomic motion in space and time in pump–probe diffraction requires a probing wavelength shorter than atomic distances; in addition, the pulse duration should be shorter than the fastest dynamics of interest, i.e. tens to hundreds of femtoseconds. Pump–probe electron microscopy and diffraction [1–4] offer these capabilities, evident in a large range of recent discoveries, for example in the fields of condensed-matter physics [5–8], chemistry [9–12] or surface science [13, 14]. On the one hand, time-resolved electron diffraction with brightest/densest electron packets [15] aims for single-shot imaging of macromolecular dynamics at hundreds-of-femtosecond resolution [16]; this requires compensation of space charge broadening with microwave-based compression or streaking techniques [17–19]. The finally achievable pulse duration and degree of coherence are limited by the irreversible parts of these Coulomb interactions. On the other hand, single-electron pulses [20, 21] avoid space charge effects entirely and, when combined with dispersion control [22], potentially offer few-femtosecond resolution and below, according to simulations [23–26]. This may come at the cost of sample restrictions [16], but pump–probe diffraction with single electrons was recently achieved on graphite, suggesting this concept's feasibility at least in the regime of reversible condensed-matter dynamics [27].

In the absence of space charge, the decisive matter becomes the shape and size of the initial phase space after electron generation by femtosecond photoemission. All subsequent beam manipulations, for example with magnetic lenses or temporal compression, cannot practically reduce the initial phase space volume. The physics of photoemission hence determines the best achievable compromises at target, for example between pulse duration and monochromaticity [28], between coherence and beam size [29] and between divergence and temporal distortions [30], among others [31]. A fundamental study and optimization of photoemission in the

femtosecond regime is therefore essential for advancing ultrafast imaging with electrons towards novel resolution regimes.

Here we investigate the use of two-photon photoemission instead of the commonly applied one-photon process for the ultrafast emission of diffraction-capable single-electron and few-electron pulses, generated at high repetition rate. We show that electron dispersion, incoherence and temporal distortions are all minimized simultaneously at photon energies approaching half of the photoemitter's work function. In addition, experimental optimization of emittance and emission duration becomes extremely simple in the two-photon regime, as a consequence of the nonlinear coupling between the optical pulses' peak intensity and the resulting current of femtosecond electrons.

2. Femtosecond photoemission

Ultrashort single-electron pulses are usually produced from flat metal photocathodes via photoelectric emission driven by femtosecond optical pulses at an ultraviolet wavelength [31]. While this scheme is practical and very stable [27], the energy spread of photoelectrons is typically much larger (hundreds of meV) than that of the driving laser pulses (tens of meV) [22, 32]. This causes dispersive broadening of single-electron wave packets during acceleration and propagation [32]. After a wave packet compressor [22–24], the achievable pulse duration is directly affected by the time-bandwidth product before the compressor [31]; a minimized longitudinal emittance is therefore essential for ultimate pulse durations in the few-femtosecond and maybe attosecond regimes [4]. Also, the initial electron beam typically shows significantly more transverse momentum than the generating laser pulses. This causes the electron beam to diverge and reduces the ratio of transverse coherence to beam diameter at the diffraction target, limiting the ability to resolve the larger unit cells of complex materials [29].

A main reason for these two types of phase space broadening during photoemission is mismatch between the laser's photon energy and the cathode material's work function [21] in combination with imperfections of the emitter material. In a simplified picture, the laser photons are absorbed in the metal and produce charge carriers that travel towards the surface. This, however, involves dephasing and scattering from impurities [33, 34], homogenizing the electron energy spectrum and directions over all available phase space. Ejection into free space occurs for such carriers, or parts of their wave function, that have enough energy exceeding the material's work function. In the single-electron regime, the emitted wave packet hence covers all the energetically available phase space continuously [21]; simply speaking, the laser's temporal and spatial coherence are lost in the photoemission process. The lower the difference between work function and photon energy, the lower is the increase of emittance when converting photons to electrons using photoemission from realistic metal surfaces.

In summary, there are three conditions for optimizing a photoemission-based femtosecond single-electron source. First, the photon energy should be close to the work function for avoiding excess bandwidth [21]. Second, the photoemission time, i.e. laser pulse width, should be optimized as a compromise between shortest duration and smallest bandwidth, using Fourier-limited optical pulses [21, 22]. Third, the area and angular spread of the photoemission process should be minimized for maximizing transverse coherence [29].

3. Two-photon photoemission

These three conditions are difficult to realize in an experiment. First, production of ultrashort and wavelength-tunable laser pulses is challenging in the ultraviolet [35–37], especially for high repetition rates in the hundreds of kHz regime. Second, minimizing the duration of photoemission requires chirp compensation at the location of the photocathode, i.e. in a vacuum environment, where optical pulse metrology is difficult. Characterizing the electron pulses themselves using laser-based streaking [32] or ponderomotive scattering [38, 39] is not routinely applicable in many laboratories. Third, minimizing the emission area to μm-sized diameters [27] is also difficult, because time-consuming waist scans with a well-aligned magnetic lens system [40] are required for a precise determination [29].

These practical difficulties with conventional photoemission sources motivated the present research and application of a two-photon process for electron emission. Such an approach was briefly mentioned earlier [2, 27, 41, 42], but neither details were given nor were tunable pulses applied. The expected advantage of two-photon photoemission is a second-order scaling between electron generation efficiency and the optical peak intensity at the photocathode material. The shorter the duration and the smaller the focus, the larger an electron current is measured. This simple relation should allow finding the optimum emission conditions easily in the experiment, without resorting to temporal electron pulse characterization or waists scans.

These questions remain: what optical intensity and pulse energy is required? How to generate the optical pulses at tunable photon energies? Are there thermal contributions to the electron current? How stable is the

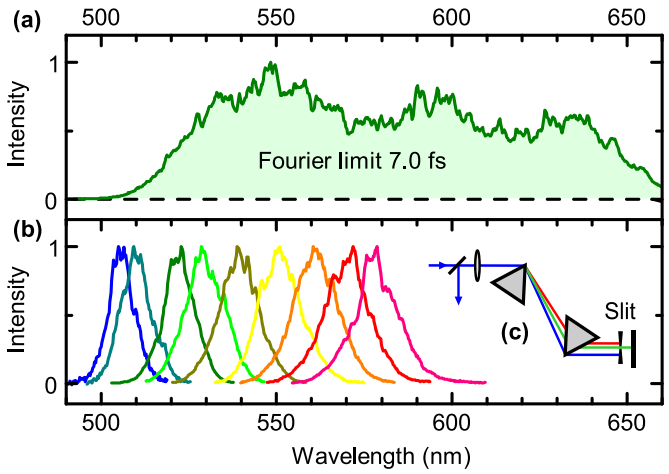

Figure 1. Performance of our NOPA system driven by picosecond pulses from an Yb:YAG disk laser. (a) Broadband output spectrum. (b) Tunable spectra with Fourier limits of ~40 fs for tunable photoemission studies. (c) Slit arrangement for spectral filtering in the Fourier domain.

current over the many hours required for a pump–probe single-electron diffraction study [27]? Is the transverse coherence comparable to conventionally generated beams [29]? What is the relation between photon excess energy and beam emittance? And finally, is two-photon photoemission a practical approach for pump–probe single-electron diffraction of reversible condensed-matter dynamics? The present letter aims at answering these questions.

4. Experimental setup—tunable visible noncollinear optical parametric amplifier (NOPA) pulses and electron beam metrology

The experimental setup consists of a picosecond laser source, a frequency conversion unit, an electron source and a diffraction beamline with single-electron area detector. The picosecond laser is a regenerative Yb:YAG thin-disk amplifier producing 330 μJ pulses at a central wavelength of 1030 nm [43], delivering 0.8 ps pulses at optimized conditions [43] and 1.0 ps in the present experiments. The laser's repetition rate is tunable between 50–400 kHz and was set to 100 kHz, appropriate for pump–probe single-electron diffraction [27]. The photocathode is a 20 nm gold layer on a sapphire substrate. Gold's work function at such conditions is about 4.3 eV [21], corresponding to an optical wavelength of 290 nm. Hence, for two-photon photoemission, we need optical pulses that are tunable in the visible spectral range around and below 580 nm. For generating these pulses, we apply a NOPA based on an earlier design [44], but specifically optimized for pumping with the picosecond pulses. A white-light continuum is difficult to achieve with long pump pulses [45], but is here successfully established using a 4 mm YAG crystal pumped with pulse energies of about 7 μJ, focused using an $f = 80$ mm lens. Similar to earlier results [46], the continuum smoothly covers the range 480–950 nm and makes an ideal seed light for the NOPA process in a 2 mm thick type-I BBO crystal at 37°. The pump pulses at 344 nm are derived from the thin-disk laser by frequency-tripling in a sequence of two group-velocity-compensating BBO crystals [44], a 0.8 mm thick type-I crystal at 23.5° for second harmonic generation followed by a 1.5 mm thick type-II crystal at 62.8° for sum-frequency mixing. Pulses are compressed using a double-pass through two fused-silica prisms with a 68.7° apex angle at a separation of ~65 cm. A dispersion-free autocorrelator [47] is applied for pulse characterization.

In this ps-driven NOPA, the ultraviolet pump pulses at 344 nm have a duration only slightly shorter than the fundamental pulses from the thin-disk laser, about 0.6–1 ps. Therefore, amplification of the chirped white-light is extremely broadband; spectra with Fourier limits down to 5.3 fs could be directly generated with a pulse energy of up to 1 μJ. This represents a factor of 150 in potential shortening of the ps-pulses from the high-power Yb:YAG disk laser. The particular spectrum used for photoemission experiments is shown in figure 1(a) and has a Fourier limit of 7 fs. In order to produce longer and tunable pulses for electron emission, some narrower parts of this spectrum are selected in the Fourier domain. To this end, the NOPA beam is focused through the two compressor prisms onto the end mirror, where an adjustable slit is located for filtering the spectrum; see figure 1(c). This selects wavelength-tunable pulses of adjustable bandwidth with energies of several nJ. Figure 1(b) shows the series of spectra applied for photoemission, continuously covering the spectral range of 505–580 nm at photon energies of 2.1–2.5 eV. The slit width is chosen to select a spectral width corresponding to

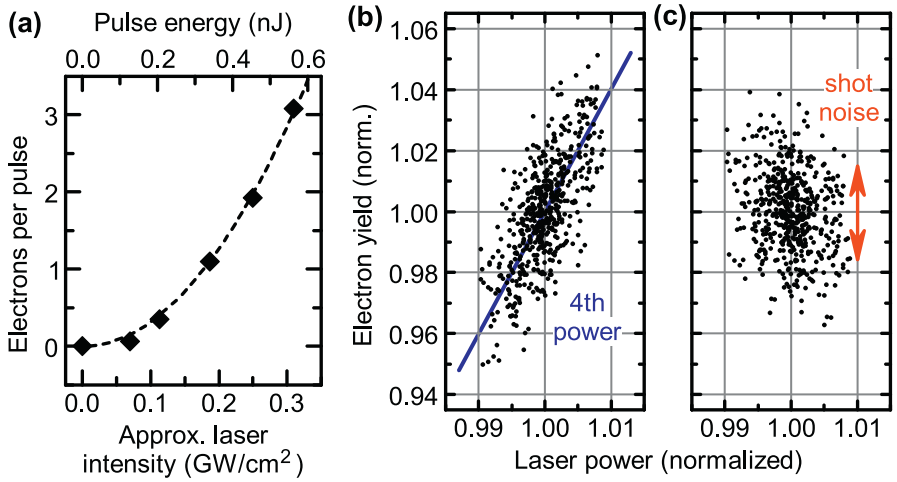

Figure 2. Two-photon photoemission at 515 nm and its stability. (a) Number of electrons per pulse obtained with varying laser pulse energy and estimated peak intensity incident on the gold layer. The clear quadratic dependence (dashed) demonstrates that two-photon photoemission is the predominant process. (b) Correlation between electron yield and fundamental laser power. The fourth-order correlation is expected from the sequence of two second-order processes, second-harmonic generation in BBO followed by two-photon photoemission at the gold layer. (c) The residual noise is uncorrelated, 1.3% rms, and limited by shot noise.

a Fourier limit of ~40 fs. The effective duration of the cathode's two-photon emission process is $\sqrt{2}$ times shorter, about 30 fs. This is close to the optimum for generating shortest electron pulses assuming high-field electrostatic acceleration (10 kV mm^{-1}) [21]. Slight adjustment of the prism compressor for each selected wavelength is sufficient to compensate the NOPA output's higher-order dispersion.

For electron generation, the optical beam is expanded to a full-width-at-half-maximum diameter of ~8 mm and sent into the electron source's vacuum chamber through a 3 mm thick fused-silica window. A $f = 35$ mm lens within the vacuum environment focuses the beam onto the photocathode, a 20 nm gold layer on the far side of a 1 mm thick sapphire substrate. The electrons are accelerated to 70 keV with an electrostatic field of ~2.8 kV mm^{-1}. The electron beam passes through an anode hole with a diameter of 8 mm. At a distance of 1.42 m, a phosphor screen and camera are used to record the electron beam for each optical central wavelength.

5. Results—quadratic emission increase and two-photon cross-section

We first show results on two-photon photoemission using sub-ps pulses at 515 nm produced directly via second-harmonic-generation at 50 kHz, and report on our findings with the tunable NOPA pulses at 100 kHz later. Figure 2(a) shows the number of emitted electrons per optical pulse in dependence on the applied peak intensity. The latter is estimated from the optical pulse duration, incident power, repetition rate, focus size and Fresnel losses of the lens and cathode substrate within the vacuum chamber. As expected, there is a quadratic dependence of the electron yield with pulse intensity. Less than 1 nJ of incident optical pulse energy is well sufficient for emitting more than one electron per pulse. Thermal effects at the photocathode are therefore negligible; this is also evident from the quadratic dependence in figure 2(a). The effective radius of the electron-emitting area is determined by knife-edge scans of the magnetically focused electron beam and by waist scans [29]; we obtain a full-width-at-half-maximum of ~8.5 μm or ~3.6 μm rms, the common definition in ultrafast electron optics [48]. This measurement is resolution-limited and the reported value is therefore an upper limit.

6. Results—stability

After about one hour of conditioning, the long-term degradation of the source is less than 1% per hour. On shorter time scales, some fluctuations originate from the thin-disk laser's output noise. Figure 2(b) shows the correlation between the optical power at 1030 nm and the electron yield taken every ten seconds over a two-hour period. The correlation coefficient is ~4, as expected from the effectively fourth-order nonlinear conversion process (unsaturated second-harmonic generation followed by two-photon photoemission). Interestingly, when removing this correlation numerically by dividing the electron yield by the fourth power of the measured optical power, there remains a residual, laser-independent noise of the electron source of 1.3% rms (see figure 2(c)). This is a consequence of shot noise. An average of 0.13 electrons were generated per pulse at a 50 kHz repetition rate and images were integrated for one second; hence there are 6500 electrons per image. Assuming that the electron emission follows Poisson statistics, the shot noise is about $\sqrt{6500}/6500 \approx 1.2\%$.

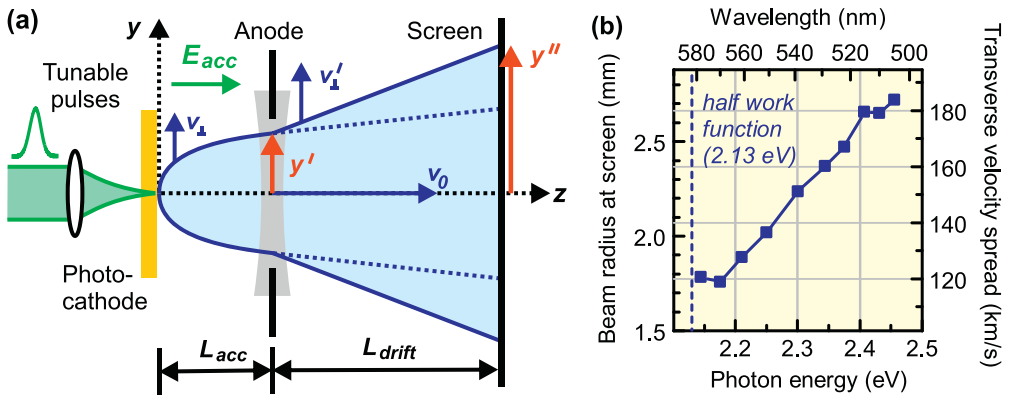

Figure 3. Experimental geometry and results on wavelength-dependent electron beam divergence. (a) Tunable femtosecond pulses from the NOPA (green) impinge on a gold photocathode (yellow). Electrons are generated by two-photon photoemission and accelerated in an electrostatic field E_{acc}. After an anode producing a defocusing lens (gray), the beam expands towards a screen. (b) Measured electron beam size and corresponding initial transverse velocity spread in dependence on the excitation wavelength and photon energy. A clear decrease towards half of the work function (dashed) indicates the superior electron beam quality obtainable with tunable NOPA pulses and two-photon photoemission.

This is very close to the measured value. We conclude that our two-photon-driven electron source operates close to the quantum-limited regime of stability when numerically compensating for the measurable slow drifts of the laser power.

7. Results—emittance and pulse duration

We next report the results with tunable NOPA pulses, aiming for a decrease of emittance when approaching half of the work function. To this end we measured the direct, unfocused electron beam radius as a function of the photoemission pump wavelength. Using the tunable pulses of figure 1(b), we obtain the beam results shown in figure 3(b), left scale. Immediately evident is a clear shrinkage of the beam size with decreasing photon energy, demonstrating a reduction of emittance when less excess energy is available. The second finding is kind of a threshold when approaching the work function; no beam smaller than ~1.8 mm radius could be generated with our system.

Before we discuss these results, we deduce from the measured beam radius y'' on the screen the photocathode's transverse momentum spread and emittance. We consider a non-relativistic approximation and the geometry depicted in figure 3(a). The optical focus size (a few μm) is negligible compared to the beam radius at the screen, millimeters. An electron emitted with a transverse velocity component $v_\perp$ moves along a parabolic trajectory in the cathode-anode region (L_{acc}) and later along a linear trajectory in the drift region (L_{drift}). The anode hole has a defocusing effect on the electron beam that can be approximated with a focal length of $f \approx -4L_{acc}$ [32]. In our experiment, $L_{acc} \approx 25$ mm, $E_{acc} \approx 2.8$ kV mm^{-1} and $L_{drift} \approx 1.42$ m. The forward velocity after acceleration is $v_0 \approx 0.47\,c$.

Let us calculate the relation between initial transverse velocity $v_\perp$ and the point of incidence y'' at the screen in a non-relativistic approximation. In the cathode-anode region, the acceleration is eE_{acc}/m_e. The time t_{acc} that an electron spends in the anode-cathode region is $t_{acc} \approx \sqrt{2m_e L_{acc}^2/(eE_{acc})}$, about 300 ps in our experiment. The small variations of t_{acc} that are caused by the initial distribution of forward velocities amount to less than one picosecond and are therefore neglected. After t_{acc}, the position y' of the electron at the anode plane is $y' \approx v_\perp t_{acc}$. The anode hole's defocusing effect ($f \approx -4L_{acc}$) and the further beam propagation over a distance L_{drift} can be described by ray transfer matrices. At the screen, the final position y'' and the transverse velocity $v_\perp''$ are given by

$$\begin{pmatrix} y'' \\ v_\perp''/v_0 \end{pmatrix} = \underbrace{\begin{pmatrix} 1 & L_{drift} \\ 0 & 1 \end{pmatrix}}_{\text{free drift}} \underbrace{\begin{pmatrix} 1 & 0 \\ 1/4L_{acc} & 1 \end{pmatrix}}_{\text{anode hole}} \underbrace{\begin{pmatrix} y' \\ v_\perp/v_0 \end{pmatrix}}_{\text{before anode}}. \quad (1)$$

Inserting the basic quantities of the experimental geometry, we obtain

$$y'' = \left[\sqrt{\frac{2m_e L_{\mathrm{acc}}^2}{eE_{\mathrm{acc}}}}\left(1 + \frac{L_{\mathrm{drift}}}{4L_{\mathrm{acc}}}\right) + \frac{L_{\mathrm{drift}}}{v_0}\right] v_\perp. \tag{2}$$

This describes a linear relation between an electron's incidence point on the screen (y'') and its original transverse velocity after photoemission ($v_\perp$). Therefore, in terms of distributions, the measured radial beam profile at the screen reveals the distribution of transverse velocities at the photocathode. A measured radius of the beam is hence directly converted to the spread of transverse velocity at the electron emitter. The results are shown in figure 3(b) with the right-hand scale.

These results, including trend and order-of-magnitude, compare very favorably to the one-photon data of Aidelsburger and co-workers [21]. For a photon energy close to the work function, or here half of the work function, emittance is reduced: shorter, more coherent and less spatiotemporally distorted electron pulses are produced. Assuming that the longitudinal velocity spread is similar to the transverse one [21], i.e. a half-spherical initial shape of the initial phase space, sub-100 fs pulses are achievable with 10 kV mm^{-1} electrostatic acceleration [21] without requiring microwave compression [22] and advanced synchronization [28]. More importantly, if single-electron pulse compression is applied with time-dependent microwave fields [22], any smaller phase space volume in the time/energy domain before compression either implies an improved monochromaticity or shorter pulses at target [22].

Transverse emittance determines the ability of electron diffraction to resolve atomic motion within complex unit cells, because only such atoms can mutually interfere that are not separated by significantly more than one coherence length. Nano-scale needle emitters are ideal in that aspect, but suffer from spatiotemporal correlations in the beam profile [50, 51] making pulse compression difficult. It is possible to apply apertures to dense electron pulses for improving coherence, but this implies space charge effects before the aperture that in part irreversibly reduce the ability for temporal compression. Our two-photon source's transverse normalized emittance is $\varepsilon_\perp = c^{-1}\sigma_\perp v_\perp$ with $\sigma_\perp$ and $v_\perp$ as rms values [48]. Assuming that the NOPA pulses at the optimum wavelength of 570 nm are focusable down to a full width of 5 μm (~4 μm $1/e^2$-radius or ~2.1 μm rms) at the gold layer, similar to what is achievable with 400 nm pulses [27], we expect an effective source size of ~1.5 μm rms and an emittance of $\varepsilon_\perp \approx 0.6$ nm. This is as good as our recently reported one-photon-driven ultrafast single-electron source [27] with coherences exceeding biomolecular dimensions [29], but here without any difficulties in reaching these values experimentally, namely without repetitive waist scans or electron pulse metrology. There are no significant spatiotemporal distortions or space-charge-induced emittance increases, hence we expect compressibility of the electron pulses to the few-femtosecond, potentially attosecond regime of duration [22, 31].

Intriguing to us is the apparent threshold of transverse velocity spread when approaching half of the work function. The measured 120 km s^{-1} rms corresponds to an energy bandwidth of 0.04 eV. This residual spread and threshold might potentially originate from an inhomogeneous distribution of effective work functions, contributions by gold's Fermi velocity, surface roughnesses, inhomogeneous distributions of initial acceleration trajectories, or from the femtosecond emission duration via the uncertainty relation. Further theoretical considerations are required here [49]. The optical pulse energy of ~0.3 nJ required for emitting one electron per pulse (see figure 2(a)) corresponds to $\sim 8 \times 10^8$ photons. About half of these are absorbed in gold and produce in the excited volume a density of hot charge carriers of $\sim 10^{21}$ cm^{-3}; this is significant as compared to the metal's basic charge density. Nevertheless, our results show that the corresponding screening and scattering processes during femtosecond photoemission are insignificant for the emittance and energy distribution of two-photon emitted single electrons.

8. Conclusions

In conclusion, an optimized NOPA produces energetic pulses with a 7 fs Fourier limit even with picosecond-long pump pulses. More narrowband tunable pulses are generated by limiting the spectrum in the Fourier plane of the prism compressor. For generating femtosecond electron pulses, two-photon photoemission is found superior to the one-photon emission process used so far in our laboratory [4]. The practical advantages are an easy optimization of optical pulse duration and focus diameter directly at the site of electron generation within the vacuum system. Temporal electron pulse metrology and waist scans can be avoided. In addition, the experiment becomes significantly simpler. First, one optical frequency conversion stage is replaced by a bandwidth-free process *in situ* at the photocathode. Second, the optical pulses can be longer, since the duration of electron emission is intrinsically reduced by about $\sqrt{2}$. Third, the effective emission area is by a factor of two smaller than the optical focus, alleviating the need for high-quality UV optics within the vacuum system. Fourth,

the direct correlation of electron yield to laser power drifts without thermal contributions or saturation effects can effectively provide a short-term and long-term stability approaching the shot noise limit, without particular efforts for laser stabilization.

The general results, namely that the transverse momentum spread with two-photon photoemission is similar to that of single-photon emission at twice the photon energy, and that emittance decreases towards half of the work function with an evident threshold, should contribute to better understanding photoemission in general, for the benefit of a wide range of applications including particle acceleration, electron microscopy or quantum optics with electrons.

Acknowledgments

We thank Dagmar Frischke for help with gold coating. We acknowledge funding from the European Research Council, DFG-Cluster of Excellence: Munich-Centre for Advanced Photonics, and the Rudolf-Kaiser Foundation.

References

[1] Flannigan D J and Zewail A H 2012 4D electron microscopy: principles and applications *Acc. Chem. Res.* **45** 1828–39
[2] Sciaini G and Miller R J D 2011 Femtosecond electron diffraction: heralding the era of atomically resolved dynamics *Rep. Prog. Phys.* **74** 096101
[3] Shorokhov D and Zewail A H 2008 4D electron imaging: principles and perspectives *Phys. Chem. Chem. Phys.* **10** 2879–93
[4] Baum P 2014 Towards ultimate temporal and spatial resolutions with ultrafast single-electron diffraction *J. Phys. B: At. Mol. Opt. Phys.* **47** 124005
[5] Baum P, Yang D S and Zewail A H 2007 4D visualization of transitional structures in phase transformations by electron diffraction *Science* **318** 788–92
[6] Eichberger M, Schafer H, Krumova M, Beyer M, Demsar J, Berger H, Moriena G, Sciaini G and Miller R J D 2010 Snapshots of cooperative atomic motions in the optical suppression of charge density waves *Nature* **468** 799–802
[7] Liu H, Kwon O-H, Tang J and Zewail A H 2014 4D imaging and diffraction dynamics of single-particle phase transition in heterogeneous ensembles *Nano Lett.* **14** 946–54
[8] Morrison V R, Chatelain R P, Tiwari K L, Hendaoui A, Bruhács A, Chaker M and Siwick B J 2014 A photoinduced metal-like phase of monoclinic VO_2 revealed by ultrafast electron diffraction *Science* **346** 445–8
[9] Ihee H, Lobastov V A, Gomez U M, Goodson B M, Srinivasan R, Ruan C Y and Zewail A H 2001 Direct imaging of transient molecular structures with ultrafast diffraction *Science* **291** 458–62
[10] Srinivasan R, Feenstra J S, Park S T, Xu S J and Zewail A H 2005 Dark structures in molecular radiationless transitions determined by ultrafast diffraction *Science* **307** 558–63
[11] Hensley C J, Yang J and Centurion M 2012 Imaging of isolated molecules with ultrafast electron pulses *Phys. Rev. Lett.* **109** 133202
[12] Gao M *et al* 2013 Mapping molecular motions leading to charge delocalization with ultrabright electrons *Nature* **496** 343–6
[13] Wall S, Krenzer B, Wippermann S, Sanna S, Klasing F, Hanisch-Blicharski A, Kammler M, Schmidt W G and Horn-von Hoegen M 2012 Atomistic picture of charge density wave formation at surfaces *Phys. Rev. Lett.* **109** 186101
[14] Park S T, Yurtsever A, Baskin J S and Zewail A H 2013 Graphene-layered steps and their fields visualized by 4D electron microscopy *Proc. Natl Acad. Sci. USA* **110** 9277–82
[15] Siwick B J, Dwyer J R, Jordan R E and Miller R J D 2002 Ultrafast electron optics: propagation dynamics of femtosecond electron packets *J. Appl. Phys.* **92** 1643–8
[16] Miller R J D 2014 Femtosecond crystallography with ultrabright electrons and x-rays: capturing chemistry in action *Science* **343** 1108–16
[17] Oudheusden T V, Pasmans P L E M, Geer S B V D, Loos M J D, Wiel M J V D and Luiten O J 2010 Compression of subrelativistic space-charge-dominated electron bunches for single-shot femtosecond electron diffraction *Phys. Rev. Lett.* **105** 264801
[18] Kassier G H, Erasmus N, Haupt K, Boshoff I, Siegmund R, Coelho S M M and Schwoerer H 2012 Photo-triggered pulsed cavity compressor for bright electron bunches in ultrafast electron diffraction *Appl. Phys.* B **109** 249–57
[19] Scoby C M, Li R K, Threlkeld E, To H and Musumeci P 2013 Single-shot 35 fs temporal resolution electron shadowgraphy *Appl. Phys. Lett.* **102** 023506
[20] Lobastov V A, Srinivasan R and Zewail A H 2005 Four-dimensional ultrafast electron microscopy *Proc. Natl Acad. Sci. USA* **102** 7069–73
[21] Aidelsburger M, Kirchner F O, Krausz F and Baum P 2010 Single-electron pulses for ultrafast diffraction *Proc. Natl Acad. Sci. USA* **107** 19714–9
[22] Gliserin A, Apolonski A, Krausz F and Baum P 2012 Compression of single-electron pulses with a microwave cavity *New J. Phys.* **14** 073055
[23] Fill E, Veisz L, Apolonski A and Krausz F 2006 Sub-fs electron pulses for ultrafast electron diffraction *New J. Phys.* **8** 272
[24] Veisz L, Kurkin G, Chernov K, Tarnetsky V, Apolonski A, Krausz F and Fill E 2007 Hybrid dc–ac electron gun for fs-electron pulse generation *New J. Phys.* **9** 451
[25] Baum P and Zewail A H 2007 Attosecond electron pulses for 4D diffraction and microscopy *Proc. Natl Acad. Sci. USA* **104** 18409–14
[26] Hansen P, Baumgarten C, Batelaan H and Centurion M 2012 Dispersion compensation for attosecond electron pulses *Appl. Phys. Lett.* **101** 083501
[27] Lahme S, Kealhofer C, Krausz F and Baum P 2014 Femtosecond single-electron diffraction *Struct. Dyn.* **1** 034303
[28] Gliserin A, Walbran M and Baum P 2013 Passive optical enhancement of laser-microwave synchronization *Appl. Phys. Lett.* **103** 031113
[29] Kirchner F O, Lahme S, Krausz F and Baum P 2013 Coherence of femtosecond single electrons exceeds biomolecular dimensions *New J. Phys.* **15** 063021

[30] Weninger C and Baum P 2012 Temporal distortions in magnetic lenses *Ultramicroscopy* **113** 145–51
[31] Baum P 2013 On the physics of ultrashort single-electron pulses for time-resolved microscopy and diffraction *Chem. Phys.* **423** 55–61
[32] Kirchner F O, Gliserin A, Krausz F and Baum P 2014 Laser streaking of free electrons at 25 keV *Nat. Photonics* **8** 52–7
[33] Spicer W E 1963 Optical transitions in which crystal momentum is not conserved *Phys. Rev. Lett.* **11** 243
[34] Spicer W E 1967 Possible non-one-electron effects in fundamental optical excitation spectra of certain crystalline solids and their effect on photoemission *Phys. Rev.* **154** 385
[35] Kozma I Z, Baum P, Lochbrunner S and Riedle E 2003 Widely tunable sub-30 fs ultraviolet pulses by chirped sum frequency mixing *Opt. Express* **11** 3110–5
[36] Baum P, Lochbrunner S and Riedle E 2004 Tunable sub-10 fs ultraviolet pulses generated by achromatic frequency doubling *Opt. Lett.* **29** 1686–8
[37] Bradler M and Riedle E 2014 Sub-20 fs μJ-energy pulses tunable down to the near-UV from a 1 MHz Yb-fiber laser system *Opt. Lett.* **39** 2588–91
[38] Hebeisen C T, Ernstorfer R, Harb M, Dartigalongue T, Jordan R E and Miller R J D 2006 Femtosecond electron pulse characterization using laser ponderomotive scattering *Opt. Lett.* **31** 3517–9
[39] Hebeisen C T, Sciaini G, Harb M, Ernstorfer R, Dartigalongue T, Kruglik S G and Miller R J D 2008 Grating enhanced ponderomotive scattering for visualization and full characterization of femtosecond electron pulses *Opt. Express* **16** 3334–41
[40] Kreier D, Sabonis D and Baum P 2014 Alignment of magnetic solenoid lenses for minimizing temporal distortions *J. Opt.* **16** 075201
[41] Wytrykus D, Centurion M, Reckenthaeler P, Krausz F, Apolonski A and Fill E 2009 Ultrashort pulse electron gun with a MHz repetition rate *Appl. Phys.* B **96** 309–14
[42] Yang D-S, Mohammed O F and Zewail A H 2010 Scanning ultrafast electron microscopy *Proc. Natl Acad. Sci. USA* **107** 14993–8
[43] Schneider W, Ryabov A, Lombosi C S, Metzger T, Major Z S, Fülöp J A and Baum P 2014 800-fs, 330-μJ pulses from a 100-W regenerative Yb:YAG thin-disk amplifier at 300 kHz, and THz generation in $LiNbO_3$ *Opt. Lett.* **39** 6604–7
[44] Homann C, Schriever C, Baum P and Riedle E 2008 Octave wide tunable UV-pumped NOPA: pulses down to 20 fs at 0.5 MHz repetition rate *Opt. Express* **16** 5746–56
[45] Bradler M, Baum P and Riedle E 2009 Femtosecond continuum generation in bulk laser host materials with sub-μJ pump pulses *Appl. Phys.* B **97** 561–74
[46] Riedel R, Stephanides A, Prandolini M J, Gronloh B, Jungbluth B, Mans T and Tavella F 2014 Power scaling of supercontinuum seeded megahertz-repetition rate optical parametric chirped pulse amplifiers *Opt. Lett.* **39** 1422–4
[47] Kozma I Z, Baum P, Schmidhammer U, Lochbrunner S and Riedle E 2004 Compact autocorrelator for the online measurement of tunable 10 femtosecond pulses *Rev. Sci. Instrum.* **75** 2323–7
[48] Geer S B V D, Loos M J D, Vredenbregt E J D and Luiten O J 2009 Ultracold electron source for single-shot, ultrafast electron diffraction *Microsc. Microanal.* **15** 282–9
[49] Jensen K L, O'Shea P G, Feldman D W and Moody N A 2006 Theoretical model of the intrinsic emittance of a photocathode *Appl. Phys. Lett.* **89** 224103
[50] Paarmann A *et al* 2012 Coherent femtosecond low-energy single-electron pulses for time-resolved diffraction and imaging: a numerical study *J. Appl. Phys.* **112** 113109
[51] Hoffrogge J, Stein J P, Krüger M, Förster M, Hammer J, Ehberger D, Baum P and Hommelhoff P 2014 Tip-based source of femtosecond electron pulses at 30 keV *J. Appl. Phys.* **115** 094506